New insights into the reactivity of the triscyclopentadienyl monothiolate uranium(IV) complexes: CS2 and CO2 insertion and redox properties. A DFT theoretical approach

Farida Kias, Soraya Abtouche, Anissa Amar, Aziz Elkechai, Abdou Boucekkine, Michel Ephritikhine

New Insights into the Reactivity of the Triscyclopentadienyl Monothiolate Uranium(IV) Complexes: CS_2 and CO_2 Insertion and Redox Properties. A DFT Theoretical Approach.

Farida Kias[a], Soraya Abtouche[b], Anissa Amar[a], Aziz Elkechai[a]*, Abdou Boucekkine[c]*, and Michel Ephritikhine[d]

[a]*Laboratoire de Physique et Chimie Quantiques, Faculté des Sciences, Université Mouloud Mammeri de Tizi-Ouzou, 15000 Tizi-Ouzou, Algeria.*

[b]*Laboratoire de Physicochimie Théorique et Chimie Informatique, Faculté de Chimie, Université des Sciences et de la Technologie Houari Boumediene (USTHB), Alger, Algeria.*

[c]*Univ Rennes, ISCR, UMR 6226 CNRS, Campus de Beaulieu, 35042 Rennes Cedex, France.*

[d]*NIMBE, CEA, CNRS, Université Paris-Saclay, CEA-Saclay, F-91191 Gif-sur-Yvette, France*

*** Corresponding authors:**

E-mail address: A.B. abdou.boucekkine@univ-rennes1.fr

A.E. aziz.elkechai@ummto.dz

Abstract

The structural properties of a series of triscyclopentadienyl monothiolate uranium(IV) complexes [U(Cp)$_3$(SR)] (Cp = η^5–C_5H_5; R = Me (**1**), ^{i}Pr (**2**), Ph (**3**), ^{t}Bu (**4**)) as well as their reactions with CO_2 or CS_2 leading to their insertion into the U–S bond, have been investigated, using relativistic Density Functional Theory (DFT) calculations. The computed activation barriers of these reactions show that insertion of CO_2 into the U–S bond of the thiolate complexes is easier and faster than that of CS_2, in agreement with the experimental observation. The study brings to light the electrostatic interactions and steric hindrance effects that play an important role in these processes. The present study aimed also to explore the redox behavior of the thiolate [U(Cp)$_3$(SR)] complexes permitting to find a very nice linear correlation (R^2 = 0.99) between the computed electron affinities and the experimental reduction half–wave potentials $E_{1/2}$. This correlation allowed to estimate the reduction potentials of [U(Cp)$_3$(SMe)] (**1**) and [U(Cp)$_3$(S^{t}Bu)] (**4**) for which the electrochemical measurement failed. Several population analyses were carried out, among them Nalewajski–Mrozek Bond Orders (NMBO) and Hirshfeld charges Analysis (HA) allowing to rationalize the insertion reactions and redox processes and to highlight the driving role of the uranium 5f orbitals.

Keywords: DFT; Thiolate Uranium(IV) Complexes; CO_2 and CS_2 activation; Insertion reactions; Redox properties; Electron affinity.

GRAPHICAL ABSTRACT

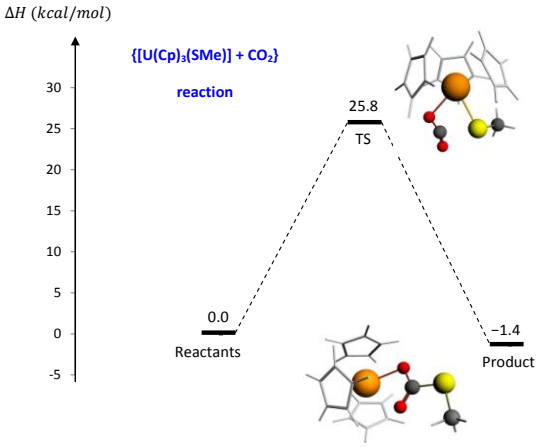

Energy profile of {[U(Cp)3(SMe)] + CO2} reaction

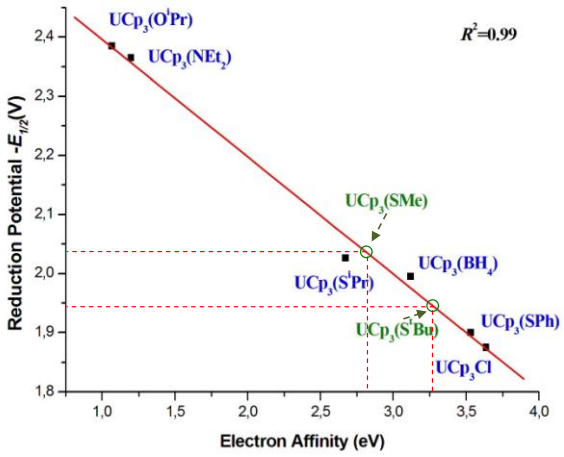

1. Introduction

The uranium chemistry constitutes, for the industrial and academic researchers, a large field of investigations not only in the domain of the nuclear fuel and the reprocessing of nuclear wastes, but also for the rich diversity of the properties and reactivity of uranium complexes [1–10]. Among them the ability of uranium complexes to undergo various redox reactions and to form a large variety of compounds with interesting structural features has been largely investigated [11–34].Another subject of study is the activation of strong bonds by uranium complexes bringing to light their potential catalytic ability. In this context, Castro and collaborators [35], studied theoretically the mechanism of reaction of the $(MeC_5H_4)_3U$ complex with the isoelectronic heteroallenes CS_2, COS, PhN_3 and PhNCO, by using DFT calculations. The obtained results were in excellent agreement with the experimental observations [11]. It was shown in particular that the difference in reactivity between CS_2 and COS is related to the difference in kinetic stability of the two molecules, CS and CO, formed during the α–abstractions starting from the bimetallic complexes $[\{(MeC_5H_4)U_3\}_2][\mu-\eta^1:\eta^2-CS_2]$ and $[\{(MeC_5H_4)U_3\}_2][\mu-\eta^1:\eta^1-COS]$ respectively. All these reactions presented a similar mechanism [17]. In 2005, an experimental study of Castro–Rodriguez and Meyer [36] showed that the highly reactive, six–coordinate tris–aryloxide U(III) species, $[(({}^t\text{BuArO})_3\text{tacn})U]$ (tacn = triazacyclononane = $(C_2H_4NH)_3$) reacts with CO_2 in a $2e^-$ reduction to produce CO and a dinuclear U(IV/IV) μ–oxygen bridged complex $[\{(({}^t\text{BuArO})_3\text{tacn})U\}_2(\mu\text{–O})]$. The authors specified that this reaction proceeds via a dinuclear CO_2–bridged intermediate. In the experimental study of Tsoureas et al. [37] carried out in 2014, related to the reductive activation of CO_2 by mixed sandwich uranium(III) complexes, it is shown that the selectivity in the outcome of CO_2 reductive activation by these complexes is steric in origin rather than electronic. The latter conclusions were supported by a detailed computational DFT study of the mechanistic pathways for the CO_2 reduction by this system [37].

However, studies of the U–S bond activation of the actinide thiolate complexes by inert small molecules such CO_2 and CS_2 remain rare. If the metal–sulfur (M–S) bond was ignored for a long time, the detection of its presence in 1982 in an active site of the metalloproteinase [38] allowed developing the chemistry of thiolate and sulfide complexes of transition metals used in bioinorganic chemistry, in the study of the nitrogenases [39], and in oil desulfurization processes [40].

The syntheses of several uranium thiolate complexes which followed transition metals ones [41–47] showed the great affinity between the uranium and sulfur atoms. Ephritikhine and Coll. studied the reactivity of the triscyclopentadienyl complex $[U(Cp)_3(S^iPr)]$ (Cp = C_5H_5) with carbon dioxide leading to the first compound resulting from the insertion of CO_2 into the U–S bond, i.e. $[U(Cp)_3(O_2CS^iPr)]$ [14,48]. In this study, some reactions of the monothiolate compounds, in particular their reduction to give the first characterized U(III) thiolates, are described, and also the synthesis of the first selenolate compounds of a 5f element. The thiolate complexes were shown to be useful precursors for the preparation of new derivatives, in particular by insertion of heteroallenes into the U–S bond.

Our relatively recent theoretical study carried out on a series of bispentamethylcyclopentadienyl bisthiolate uranium(IV) $[U(Cp^*)_2(SR)_2]$ (R = Me, ^{i}Pr, Ph and ^{t}Bu) [49] and their reactions with CO_2 and CS_2 show that the insertion of CO_2 into the U–S bond of these complexes is easier than that of CS_2. This study revealed the significant role played by the steric and electronic factors of the R ligands in the reactivity of the bisthiolate complexes of U(IV). Moreover, the better reactivity of carbon dioxide is explained by the greatest electronegativity of O allowing a good alternation of charges in the transition states, and by the well-known oxophilic character of uranium.

In addition, it is known that the redox properties of actinide complexes play a significant role in organometallic chemistry, energy and environmental science, for being involved in nuclear fuel, power plants wastes and other contamination remediation. The uranium atom can exhibit several oxidation states in complexes, from 2 to 6. However, the experimental determinations of the potentials and/or the electronic affinities (ionization energies) are rare. In this regard, theoretical computations become appealing, since their ability to successfully predict and confirm structural and redox properties of actinide–containing complexes has been shown. Thus, it seemed to us interesting to investigate the redox behavior of the thiolate complexes, with the aim of evaluating their electronic affinities and of deducing the reduction potentials of compounds not measured experimentally.

In this paper, the reactivity towards small heteroallene molecules as well as the redox properties of a series of triscyclopentadienyl thiolate uranium(IV) complexes, are investigated using relativistic DFT calculations. Four monothiolate complexes, *i.e.* $[U(Cp)_3(SMe)]$ (**1**), $[U(Cp)_3(S^iPr)]$ (**2**), $[U(Cp)_3(SPh)]$ (**3**) and $[U(Cp)_3(S^tBu)]$ (**4**) are considered. Their structures are depicted in Figure 1. First, we shall focus our attention on the insertion of CO_2 and CS_2 into the uranium–sulfur bond in order to explain the difference in reactivity of the thiolate

compounds with these small molecules. Indeed, it is observed experimentally that the insertion of CO_2 in the U–S bond of the thiolate complexes is easier and faster than that of CS_2, and it is our aim to explain why. Special attention will be devoted to the electronic and steric properties of the R group attached to the sulfur atom which drive the reactivity of the U(IV) complexes under consideration. Key features of the electronic and geometric structures should reveal further insights into the interaction of uranium thiolate complexes with small heteroallenes. Thus, Nalewajski–Mrozek bond orders (NMBO) [50], Mulliken population (MPA) [51] and Hirshfeld charges (HA) [52] analyses will be used to characterize the bonding and electronic structure of the considered species.

In a second part, the redox properties of this series of monothiolate uranium complexes, addressed in terms of electron affinity (EA) and reduction potentials ($E_{1/2}$), are explored using the same theoretical method. Results of former studies [53] on the triscyclopentadienyl complexes [U(Cp)$_3$(X)] (X = Cl, BH_4, NEt_2 and O^{i}Pr) will be used in order to estimate the reduction potentials of the monothiolate complexes not determined experimentally, i.e. **1** and **4**.

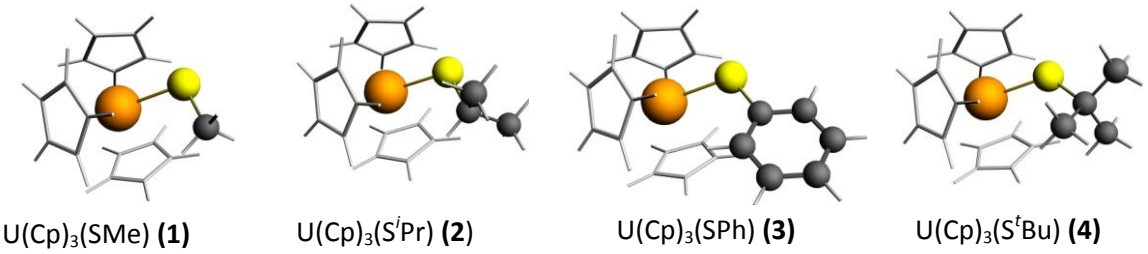

Fig. 1. Studied triscyclopentadienyl monothiolate uranium(IV) complexes

2. Computational details

The calculations were performed at the DFT level [54–56], scalar relativistic corrections being introduced via the zero–order regular approximation (ZORA) [57,58] to the Dirac equation. Solvents effects have been taken into account using the Conductor–like Screening Model (COSMO) [59,60]. Geometry optimizations, which have been carried out at the scalar relativistic level, were followed by single point computations including spin–orbit coupling when studying the redox properties of the complexes. The calculations were performed using the Amsterdam Density Functional (ADF2017.103) program package [61]**.** The Vosko–Wilk–Nusair functional (VWN) [62] for the local density approximation (LDA) and the gradient

corrections for exchange and correlation of Becke and Perdew [63–65] respectively, i.e. the BP86 functional have been used. Triple–ζ Slater–type basis set (STO) augmented by one set of polarization functions, i.e. the triple–zeta polarized (TZP) basis set, taken from the ADF/ZORA/TZP database directory, were used for all atoms. The more extended ZORA/TZ2P basis set has also been used to check the accuracy of the computed properties. The frozen–core approximation, where the core density is obtained from four–component Dirac–Slater calculations, has been applied for all atoms. For carbon C.1s, oxygen O.1s, and nitrogen N.1s, the 1s core electrons were frozen, while the 1s/2s/2p cores were frozen respectively for the chlorine Cl.2p and sulfur S.2p. The U.5d valence space of the heavy element includes the 5f/6s/6p/6d/7s/7p shells (14 valence electrons). The spin unrestricted DFT scheme is used. An integration parameter of 6.0 was applied for the geometry optimizations. Several studies have shown that the ZORA/BP86/TZP approach reproduces the experimental geometries and ground states properties of f–element compounds with a satisfying accuracy [66–70].

In this study, we carried out first the full geometry optimizations in the gas phase then the geometries were re–optimized in the solvent (benzene, toluene or THF) using the COSMO model. All geometry optimizations were carried out without any symmetry constraint. We used the non–default Delley type of cavity, with the solvent being considered with its dielectric constant and its cavity radii. Then, single–point calculations including spin–orbit corrections were carried out using the previously optimized geometries for both the gas phase and the solution. In our case of open–shell systems, the non–collinear approximation has been used [71]. Molecular geometry and molecular orbital plots were generated, respectively, by using the MOLEKEL [72] and the ADFVIEW programs [61].

All obtained stationary points located on the PES were characterized as extrema that could be minima (reactants, products with a number of imaginary frequencies Nimag = 0) or first order transition states (Nimag = 1) through harmonic approximation vibration frequency calculations. The mode associated to the imaginary frequency was analyzed to ensure that the correct transition state was found. The Intrinsic Reaction Coordinate (IRC) method [73] was used to confirm the occurrence of a transition state linking the two corresponding minima (reactants, intermediates states or final products). The zero–point vibrational energy (ZPVE) corrections within the harmonic approximation were included in all reported relative energies given in kcal.mol^{-1}, obtained at a temperature of 298.15 K. The enthalpy barriers represent the enthalpy differences between the transition state and the reactant ($\Delta H^{\#}$ = $\Delta H(TS)$ −

ΔH(reactants)). Finally, the Nalewajski–Mrozek bond orders (NMBO) and Hirshfeld charges (HA) have been used to characterize the bonding and the charge transfer during the chemical reaction.

The second aim of the present work is to explore the redox behavior of the neutral monothiolate uranium(IV) complexes $[U(Cp)_3(SR)]$ (R = Me, ^{i}Pr, Ph, ^{t}Bu), through the determination of the electron affinities related to the U(III)/U(IV) systems. Since available experimental electron affinities of molecules and complexes are largely adiabatic, the most direct theoretical method consists in the calculation of the energy difference between the neutral and anionic forms of the complexes at their respective optimized geometries, i.e. the "Δ*E* method". In terms of the energies *E*, at optimized geometries, EA is computed as follows: EA = *E*(neutral) – *E*(anion) for the reduction reaction. The ADF program that we use produces Total Bonding Energies (TBE) rather than total energies, so that EA is computed in our case as the TBE(neutral) – TBE(anion) difference for the reduction process. Electron affinities are often not reachable experimentally, whereas their theoretical estimation remains a challenge for theoretical chemists because they involve open–shell systems where spin contamination and SCF convergence problems add to the difficulty of producing reliable results. For our part, spin contamination was found negligible in our computations, owing to the fact that the computed values $<S^2>$ of the squared spin operator are very close to the exact values for all the studied species (deviation less than 1%).

3. Results and discussion

3.1. Molecular geometry optimizations of the [U(Cp)₃(SR)] monothiolate complexes

The full geometry optimizations of the neutral complexes, $[U(Cp)_3(SMe)]$ (**1**), $[U(Cp)_3(S^{i}Pr)]$ (**2**), $[U(Cp)_3(SPh)]$ (**3**), $[U(Cp)_3(S^{t}Bu)]$ (**4**), were carried out at the ZORA/BP86/TZP level in the gas phase and further re–optimized in solution (THF solvent) using the COSMO approach. The non–default Delley type of cavity was used, the solvent being considered with its dielectric constant of 7.58 and a radius of 3.18 Å.

In Table 1 are reported the most relevant optimized geometrical parameters, *i.e.* metal–ligand distances and bond angles for the studied complexes computed in the gas phase, and in solution; experimental X-ray data [14] are added for complex **1** (the Cartesian coordinates are given in Supporting Information SI.1). The optimized geometries of all complexes $[U(Cp)_3(SR)]$ (R=Me, ^{i}Pr, Ph, ^{t}Bu)] are displayed on Figure 2.

Our discussion will be focused first on the optimized geometries obtained for the complexes in the gas phase. As expected, the uranium centre is found in a classical pseudo–tetrahedral bent sandwich configuration in all complexes, that is familiar for $[U(Cp)_3(X)]$ complexes [1]. The computed U–S distances of all thiolate complexes vary from 2.66 to 2.71 Å.

Table 1

Selected distances (Å) and angles (deg.) for complexes **1**–**4** optimized in the gas phase and in THF (italic red values).

Reactants	$[U(Cp)_3(SMe)]$(**1**)	$[U(Cp)_3(S^iPr]$(**2**)	$[U(Cp)_3(SPh)]$(**3**)	$[U(Cp)_3(S^tBu)]$(**4**)
U−S$_1$	2.668 **[2.695(4)]** *(2.666)*	2.667 *(2.691)*	2.704 *(2.729)*	2.674 *(2.691)*
U−Ct$_i$*	2.489 **[2.48 (1)]** *(2.484)*	2.489 *(2.488)*	2.486 *(2.483)*	2.494 *(2.493)*
<U−C(Ct$_i$)>	2.767 *(2.759)*	2.766 *(2.769)*	2.763 *(2.763)*	2.767 *(2.768)*
<C−C(Ct$_i$)>	1.420 *(1.417)*	1.419 *(1.420)*	1.420 *(1.420)*	1.419 *(1.420)*
S$_1$−C$_1$	1.849 **[1.79 (2)]** *(1.849)*	1.873 *(1.876)*	1.787 *(1.789)*	1.899 *(1.902)*
<Ct$_i$−U−Ct$_j$>	117.0 **[(117.4)]** *(117.3)*	116.7 *(116.6)*	116.8 *(116.8)*	116.0 *(115.9)*
<Ct$_i$−U−S$_1$>	92.9 **[95.6(4)]** *(94.4)*	93.4 *(93.0)*	93.0 *(93.1)*	94.2 *(94.6)*

Values in bold blue color are the X–ray values [14], available only for the SMe derivative

* Ct_i (i = 1, 2, 3) are the Cp ring centroids.

The computed U–S bond lengths of complex **1,** namely 2.668Å is in very good agreement with the X–ray value of 2.695(4) Å. In complex **1** displayed on Figure 2, the carbon atoms of each cyclopentadienyl ring are coplanar. The computed distances between the uranium atom and the centroid of the Cp rings U–C_t which average 2.49 Å reproduce correctly the value of 2.48 Å determined by X–ray crystallography, whereas those between the metal and carbon atoms of the cycle U–C_i are on average 2.76 Å long. On the other hand, the computed angles correctly reproduce those observed in the solid state; as an example, the angles S_1–U–Ct_1 and Ct_1–U–Ct_2 of 92.9 and 117.0° respectively, are very close to the X–ray values equal to 95.6 and 117.4°. Finally, as it can be seen in Table 1, the influence of the THF solvent on the op-

timized geometrical parameters of complex **1** is rather small, noting that the interatomic distances optimized in the THF solvent are closer to the X–ray ones. The good agreement obtained for complex **1** indicates that the optimized geometries of the three other complexes should be reliable.

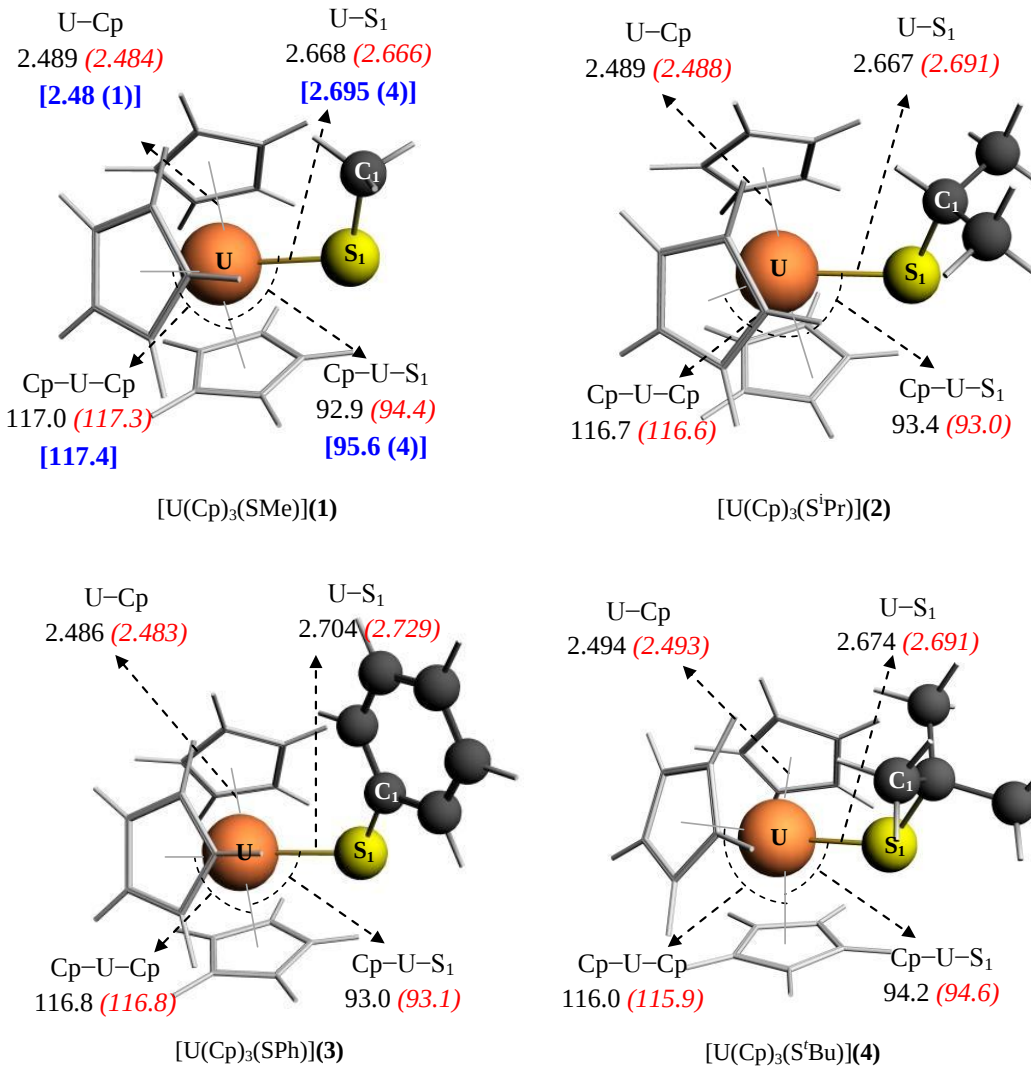

Fig. 2. Optimized geometries, obtained distances in the gas phase and in THF (between parentheses) for complexes **1** – **4**.

We consider now the Nalewajski–Mrozek Bond Orders (NMBO) that are useful tools for the analysis of bonding in organometallic complexes. Generally, calculated NMBO correlate very well with experimental properties like bond lengths and vibrational frequencies. In Table

2, are reported the computed NMBO of selected bonds and their corresponding distances in the gas phase and in solvent (in italic, between parentheses).

Table 2

NMBO of selected bonds of the monothiolate complexes **1** – **4** and CS_2 and CO_2 molecules, in the gas phase and in THF (between parentheses).

Reactants	R = Me (**1**)	R = ^{i}Pr (**2**)	R = Ph (**3**)	R = ^{t}Bu (**4**)
U−S_1	1.195 (*1.149*)	1.199 (*1.166*)	1.091 (*1.051*)	1.228 (*1.205*)
S_1−C(R)	1.016 (*1.015*)	0.955 (*0.954*)	1.076 (*1.074*)	0.918 (*0.917*)
$C(cs_2)$ −S_i*	1.996 (*1.996*)			
$C(co_2)$ −O_i*	1.970 (*1.970*)			

S_i = S_2 or S_3; O_i = O_2 or O_3

As it can be seen in Table 2, the monothiolate uranium complexes present single U–S and S–C bonds, their bond indexes being slightly higher than 1. The U–S bonds, which are involved in the insertion reaction, present bond indexes in the solvent varying from 1.051 for R = Ph to 1.205 for R = ^{t}Bu. Regarding CS_2 (or CO_2) molecule, the NMBO of C–S_i and C–O_i are all close to 2 indicating the double character of these bonds. In addition, the solvent practically does not affect the NMBO.

Mulliken Population (MPA) and Hirschfeld charges (HA) Analyses of the monothiolate uranium(IV) complexes bring light on some other aspects of the metal–ligand interactions. Despite its well know limitations, MPA permits to describe qualitatively the evolution of charge transfers and bonding interactions occurring in a series of homologous molecular systems, while the HA analysis which has been shown to be useful in inorganic chemistry, provides more reliable atomic net charges [52]. In Table 3 are collected the computed MPA and HA charges of U, S atoms and R, Cp ligands of the neutral compounds. By net charges of R and Cp, one understands the global charge of the radical and the cyclopentadienyl ligands respectively and not only that of the atom connected to uranium.

Table 3

Mulliken Populations and Hirschfeld Charges (between parentheses) Analyses of the monothiolate complexes calculated in THF.

Complexes	$[U(Cp)_3(SMe)]$	$[U(Cp)_3(S^iPr)]$	$[U(Cp)_3(SPh)]$	$[U(Cp)_3(S^tBu)]$
U	0.554 (0.528)	0.505 (0.528)	0.492 (0.536)	0.481 (0.529)
S_1	−0.236 (−0.193)	−0.217 (−0.177)	−0.188 (−0.153)	−0.127 (−0.168)
R	0.002 (0.004)	0.020 (−0.005)	−0.039 (−0.015)	−0.031 (0.004)
	−0.320 (−0.339)	−0.308 (−0.346)	−0.265 (−0.368)	−0.323 (−0.365)

The Mulliken analysis indicates that the net charges of the metal are largely smaller than its oxidation state +4 for the neutral compounds due to the ligands–to–metal donation, the latter effect being highlighted by the weak negative charges carried by the Cp and thiolate ligands.

Regarding the HA results, as already noticed with MPA, the ligand−to−metal donation is large for the U(IV) ion. The negative charges are mainly localized on the sulfur atom and the Cp ligands, noting that the sulfur atom presents a charge of −0.173 on average, largely higher than the one exhibited by the Cp ligand (−0.118 in THF on average). This result indicates that the interaction of these two entities (S and Cp) with the uranium ion that bears a positive charge equal to +0.530 in average, exhibits an electrostatic character.

3.2.Reactivity of the $[U(Cp)_3(SR)]$ complexes towards CS_2 and CO_2

Thereafter, we focus our attention on the reactivity of the considered monothiolate uranium(IV) complexes $[U(Cp)_3(SR)]$ (R = Me, ^{i}Pr, Ph, ^{t}Bu) towards the small heteroallene molecules CS_2 and CO_2. This reactivity of thiolate compounds is investigated using the methodology described below, the product of the reaction being the insertion of these molecules in the U−S bond. All stationary points on the potential energy surface have been fully optimized and were characterized, through vibration frequencies calculations, as minima without any imaginary frequency or transition states (TS) with only one imaginary frequency. The IRC calculations carried out for the $\{[U(Cp)_3(SR)] + CX_2\}$ reactions (with R = Me, ^{i}Pr, Ph, ^{t}Bu and X= S, O) showed the nonexistence of any intermediate state (IM) between the transition state and the reactants (or product). In all reactions for the considered spin state, the TS connects directly the reactants (at IRC backward) and the product (at IRC forward); it can be noticed that the product is generally more stable that the reactants (exergonic reactions).

As shown by Ephritikhine and Coll. [14], on exposure to carbon dioxide in THF (1 atm; 20°C), $[U(Cp)_3(S^iPr)]$ was in rapid equilibrium with $[U(Cp)_3(O_2CS^iPr)]$ resulting from reversible insertion of CO_2 into the uranium−sulfur bond. In contrast, the reaction of

$[U(Cp)_3(S^iPr)]$ with CS_2 was much slower and gave the trithiocarbonate $[U(Cp)_2(S_2CS^iPr)_2]$ and unidentified products. A similar study on the bisthiolate uranium (IV) complex $[U(Cp^*)_2(S^tBu)_2]$ [48] showed that it reacted very quickly (a few minutes) with CO_2 to give $[U(Cp^*)_2(O_2CS^tBu)_2]$ whereas its reaction with CS_2 required two days to form the monoinsertion product $[U(Cp^*)_2(S^tBu)(S_2CS^tBu)]$.

In the following sections the characteristics of each reaction in terms of geometries, energies, charge distributions will be detailed.

3.2.1. Reaction mechanism for the {$[U(Cp)_3(SR)]$ + CX_2} reactions

The Linear Transit (LT) calculations show that the insertion reaction of CS_2 into the U–S bond of $[U(Cp)_3(SR)]$ complexes proceeds first by the interaction of CS_2 with the methylthiolate group SR. The carbon atom of CS_2 approaches the sulfur atom of the SR ligand, then one of its C–S bond is elongated from 1.57 Å in free CS_2 to around 1.66 Å concomitantly accompanied by a bending of the molecule reaching an angle of ca. 144° in the TS structures. Meanwhile the U–S bond is elongated for R = Me from 2.668 Å in the reactant to 2.755 Å in the TS, leading to the breaking of this bond. Then, the already formed $SRCS_2^-$ ligand coordinates to the uranium atom in a η^2–SS mode leading to the formation of the insertion product $[U(Cp)_3(S_2CSR)]$ where the CS_2 molecule is inserted in the U–S bond; the two U–S(CS_2) bonds exhibit slightly different lengths, *ca*. 2.87 Å for one and 3.12 Å for the other. The geometrical parameters relative to the moieties not involved in the insertion process remain unchanged. The geometrical structure of the insertion product $[U(Cp)_3(S_2CS^tBu)]$ is displayed in Figure 3. (Cartesian coordinates of TS and products for all reactions with CS_2 are in Supporting Information SI.2).

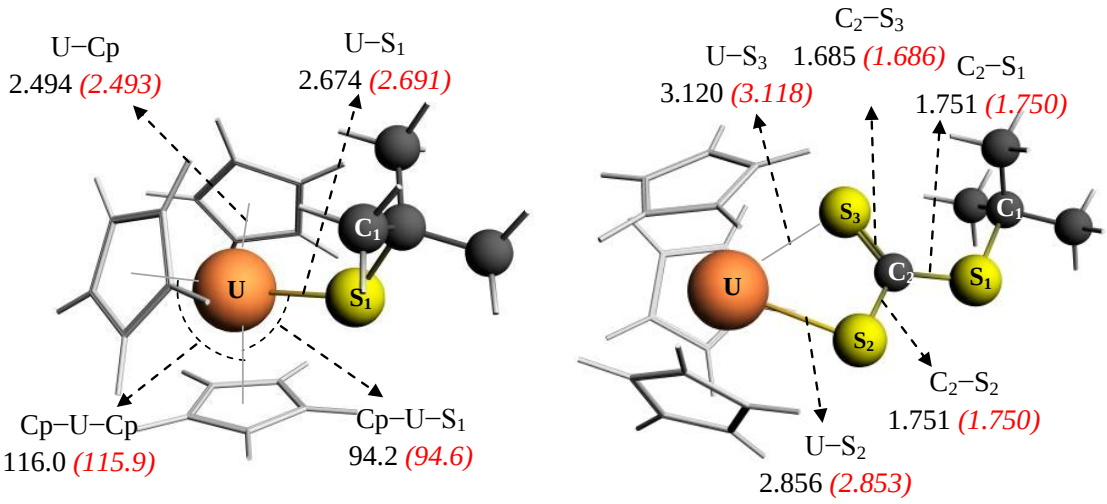

Fig. 3. Geometrical structure of the reactant (left) and the insertion derivative (right) $[U(Cp)_3(S_2CS^tBu)]$ complex (after CS_2 insertion); distances computed in gas phase and in THF (between parentheses).

The LT calculations show that the insertion reaction of CO_2 takes place in a slightly different way from that of CS_2, the CO_2 molecule being much more attracted by the uranium complex for electrostatic reasons. Indeed, the first step of the insertion is the approach of the CO_2 molecule to the $[U(Cp)_3(SR)]$ monothiolate complex that involves the electrostatic attraction between the positively charged carbon and the negatively charged sulfur, CO_2 losing its linearity to reach a O-C-O angle of about 150° in the TS(s). Then occurs the formation of the C–S bond accompanied by the elongation of the C–O bond from 1.160 Å in the free CO_2 to reach about 1.190 Å in the transition state. The uranium-oxygen bonding is characterized by the lengths of the U–O1 bond in the TS (2.509 Å for the $\{[U(Cp)_3(SMe)] + CO_2\}$ reaction and 2.466 Å for the $S^iPr–CO_2$ case), which are largely smaller than the lengths observed for the homologous reactions with CS_2, *i.e.* 2.883 and 2.811 Å respectively) as it is shown in Figure 4. Thus, the electrostatic attraction between the relevant atoms should be larger in the CO_2 case. In parallel, we observe that the U–S bond length is slightly elongated from 2.60 Å to reach 2.70 Å before breaking. The second step shows that CO_2 is inserted into the U–S bond after the coordination of the $SRCO_2^-$ ligand to the uranium ion in a η^2–OO mode by forming two slightly different U–O bonds (lengths of 2.41 Å and 2.64 Å) then leading to the final product of the reaction. The transition state and product structures of $\{[U(Cp)_3(SR)] + CX_2\}$ (R = Me, ^{i}Pr; X = S, O) reactions are displayed in Figure 4.

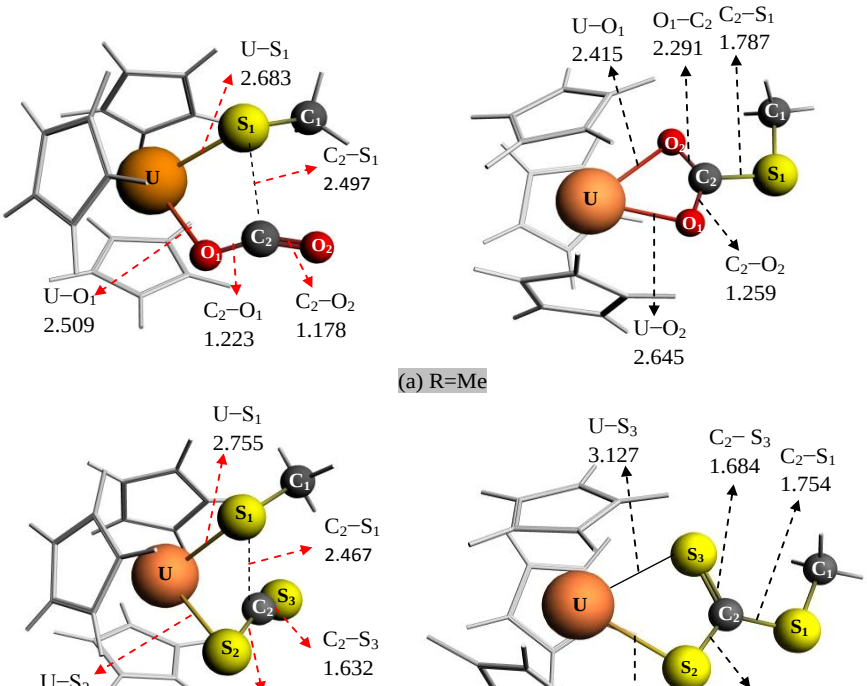

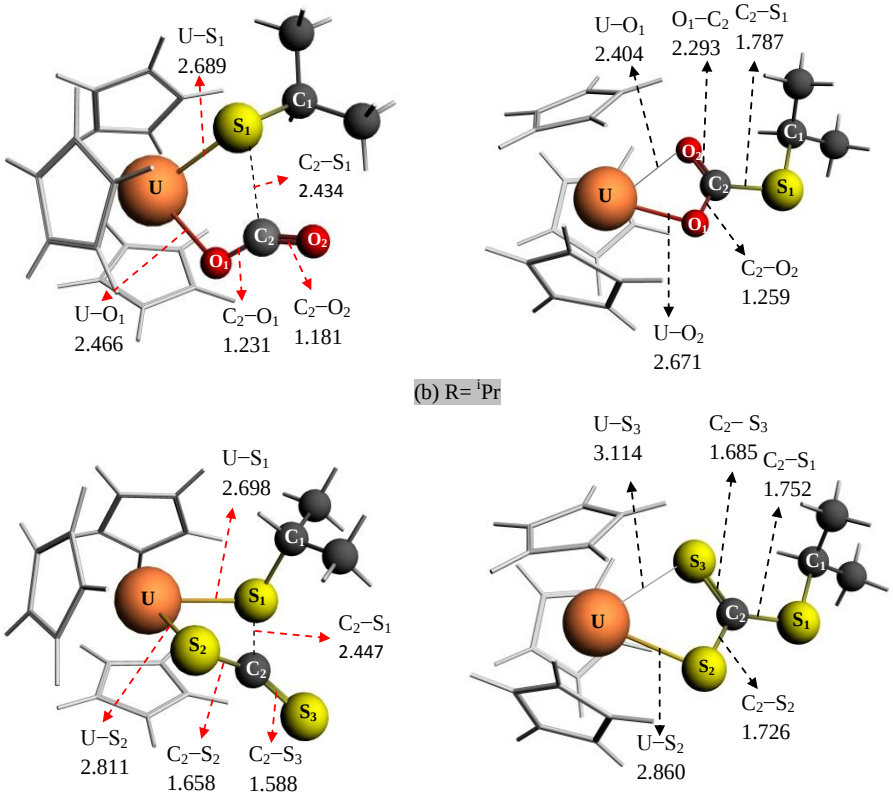

Fig. 4. Geometrical structures of the transition states (left) and products (right) of the {[U(Cp)$_3$(SR)] + CX$_2$} reactions with X = O (top) and S (bottom), and R = Me (a), ^{i}Pr (b), in THF (sulfur atoms in yellow, oxygen ones in red, carbons in green).

The energy profiles determined in the THF solvent for the two [U(Cp)$_3$(SMe)] + CS$_2$/CO$_2$ reactions are depicted in Figure 5 (a = Me with CS$_2$, b = Me with CO$_2$). The energy profiles for the other reactions (R = ^{i}Pr, Ph and ^{t}Bu), which are similar, are given in Supporting Information SI.3.

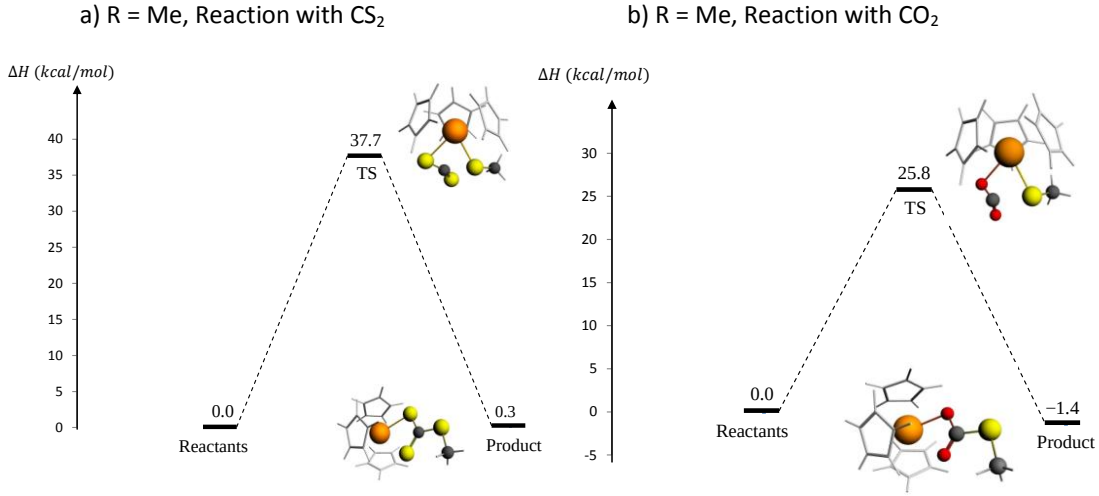

Fig. 5. Energy profiles for the {[$U(Cp)_3(SMe)$] + CS_2/CO_2} reactions in THF: (a) {[$U(Cp)_3(SMe)$] + CS_2} (b) {[$U(Cp)_3(SMe)$] + CO_2}. Energy profiles obtained in gas phase are in Supporting Information SI.4.

The reaction energy profile of the complex [$U(Cp)_3(SMe)$] reacting with CS_2 in THF (Figure 5) shows that the reactants must overcome the energy barrier of 37.7 kcal.mol^{-1} in order to proceed to the final product. In Table 4, are reported the relative enthalpy energies to the reactants of all stationary points (reactants, TS(s) and product) calculated in the gas phase and in THF. The formation of the insertion product [$U(Cp)_3(S_2CSMe)$] is then kinetically accessible compared to the other reactions (Table 4) and the enthalpy energy of the product is very close to that of the reactants(as seen in Fig 5 (part a)). The other reactions (for R = ^{i}Pr, Ph and ^{t}Bu) present larger activation energies in THF (ranging from 39.0 to 42.2 kcal.mol^{-1}).

Table 4

Relative enthalpy energies (kcal.mol^{-1}) determined in THF of stationary points at the ZORA/BP86/TZP level of theory: reactants, products and transition state of the {[$U(Cp)_3(SR)$] + CX_2} reactions (R = Me, ^{i}Pr, Ph, ^{t}Bu and X = S, O).

		Relative enthalpy ΔH (kcal.mol^{-1})		
R	X	Reactants	TS	Product
Me	S	**0**	37.7	0.3
	O	**0**	25.8	−1.4
^{i}Pr	S	**0**	39.0	0.1
	O	**0**	27.4	−2.9
Ph	S	**0**	40.8	6.2
	O	**0**	39.7	2.9
^{t}Bu	S	**0**	47.1	−1.8
	O	**0**	42.2	−9.6

The results presented in Table 4 show that the activation energies of the {[$U(Cp)_3(SR)$] + CS_2} reactions, ranging from 37.7 to 47.1 kcal.mol^{-1} in the solvent, are all greater than those of their homologous {[$U(Cp)_3(SR)$] + CO_2} reactions. For instance, the {[$U(Cp)_3$ (SMe)] + CS_2} reaction has a higher energy barrier (calculated at 37.7 kcal.mol^{-1}) than that of the

{[$U(Cp)_3(SMe)$] + CO_2} one (estimated at 25.8 kcal.mol^{-1}). In the case of R = ^{i}Pr, the difference is also larger, *i.e.* 39.0 *vs.* 27.4 kcal.mol^{-1}. This indicates that the reactions of the thiolate complexes with CO_2 are easier to carry out than those with CS_2. These results are in line with the experimental observation where the formation of the $U(Cp)_3(O_2CS^iPr)$ product occurs very quickly, i.e. after 10 minutes of reaction between $U(Cp)_3(S_iPr)$ and CO_2. For the same reaction with CS_2, 3 days are necessary to observe the formation of the observed product $[U(Cp)_2(S_2CS^iPr)_2]$. Electrostatic interactions and steric factors between the reacting species are among the driving factors.

3.2.2. Hirshfeld charges analysis of the {[U(Cp)$_3$(SR)] + CX$_2$} reactions

The HA atomic charges of the various structures (reactants, transition state and product) for the representative case of {[$U(Cp)_3(SMe)$] + CX_2} reactions (X = S, O), calculated in the THF solvent, are given in Table 6. The HA charges in the gas phase are given in Supporting Information SI.5.

Table 6

Hirshfeld charges analysis of the {[$U(Cp)_3(SMe)$] + CX_2}(with X = S, O) reactions in THF.

$U(Cp)_3(SMe) + CO_2$	**U**	**S1**	**C1**	**C2(co_2)**	**O1**	**O2**
Reactants	0.528	−0.187	−0.119	0.311	−0.155	−0.155
TS	0.537	−0.083	−0.111	0.237	−0.180	−0.135
Products	0.597	0.016	−0.109	0.133	−0.251	−0.210
$U(Cp)_3(SMe)_2 + CS_2$	**U**	**S1**	**C1**	**C2(cs_2)**	**S2**	**S3**
Reactants	0.528	−0.187	−0.119	−0.020	0.010	0.010
TS	0.464	−0.029	−0.116	−0.084	−0.006	0.036
Products	0.510	0.056	−0.112	−0.044	−0.132	−0.046

In Figure 8a are depicted the charges distributions in the case of the {[$U(Cp)_3(SMe)$] + CX_2} (X = S, O) reactions. A striking difference appears comparing the CS_2 and CO_2 approaches. The charges borne by the U and S atoms of the [$U(Cp)_3(SMe)$] complex are respectively equal to +0.528 and −0.187. The charge distribution in the CO_2 molecule, namely a

carbon atom positively charged (+0.311) and an oxygen atom negatively charged (−0.155), is well suited to interact with the uranium and sulfur atoms of the U−S bond leading to a four centre TS with U…O and C…S contacts. On the contrary, the C and S atoms of CS_2 bear opposite charges, i.e. −0.020 for C and +0.010 for S, so that the electrostatic interaction that occurs between CS_2 and the U and S atoms of the complex is not favored.

The charge distribution (Figure 8a) in the case of the{$[U(Cp)_3(SMe)]$ + CO_2} reaction shows a transition state with the carbon atom of CO_2 positively charged (+0.237), the sulfur atom S1 of the SR ligand negatively charged (−0.083), the metallic centre positively charged (+0.537) and the oxygen atom negatively charged (−0.135). On the contrary, for the reaction with CS_2, the C atom of CS_2 bears the negative charge −0.084 and S the negative charge −0.060. Thus, the TS state of the reaction with CO_2 could be more stabilized than in the case of CS_2, the ionic character of bonding in the four-centre TS structure being greater. This charge distribution is also observed in the reactants and the final product of the reaction. The evolution of the charges distributions during the reaction process is shown on Figure 8b.

Indeed, for the {$[U(Cp)_3(SMe)]$ + CO_2} reaction, the uranium charge varies from +0.528 in the reactant complex to +0.597 in the product, after the CO_2 insertion into the U−S bond. On the opposite, the identical charges of O1 and O2 atoms of CO_2, equal to −0.155, at the beginning of the reaction, vary to −0.210 and −0.251, respectively, at the end of the reaction. The S1 atom of the SMe fragment loses much of its negative charge (this charge passes from −0.193 to +0.016).

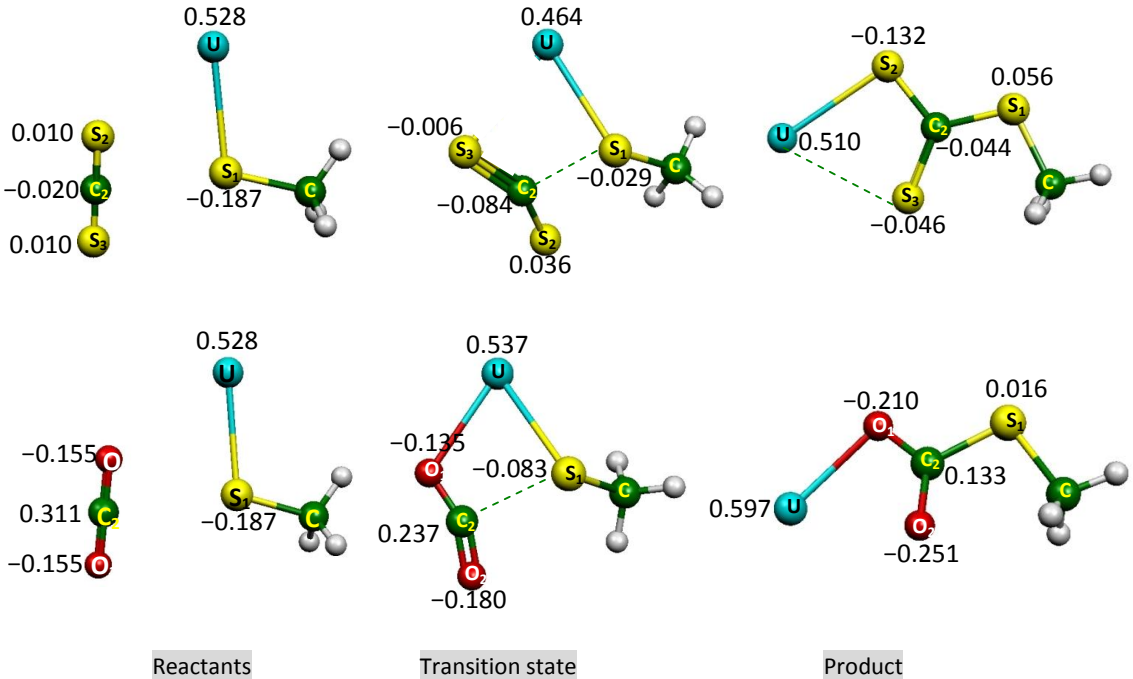

Fig. 8a. Hirshfeld atomic charges distribution of the stationary states (reactants, transition state and product) during the {[U(Cp)$_3$(SMe)] + CX$_2$} (X = S, O) reactions in THF (oxygen atoms in red, sulfur in yellow and carbon in green).

On the other hand, in the case of the reaction with the CS_2 molecule (Table 6), contrarily to the case of CO_2, the uranium charge decreases from the reactant (+0.528) to the product (+0.510). Meanwhile, the S2 and S3 atoms of initial charge +0.010 take the negative charges −0.046 and −0.132 respectively, those of the two atoms C1 and C2 remaining practically constant during the reaction. Moreover, one notes that the charge of the S1 atom of the SMe fragment (−0.187) at the beginning of the reaction) varies strongly until becoming positive (charge +0.056 in the product) in the case of the reaction with CS_2. The graphical evolution of charges (Figure 8a) and their distribution during the reaction (Figure 8b) show well the electrostatic interaction between the sulfur atom of the monothiolate complex and the molecule CS_2 /CO_2.

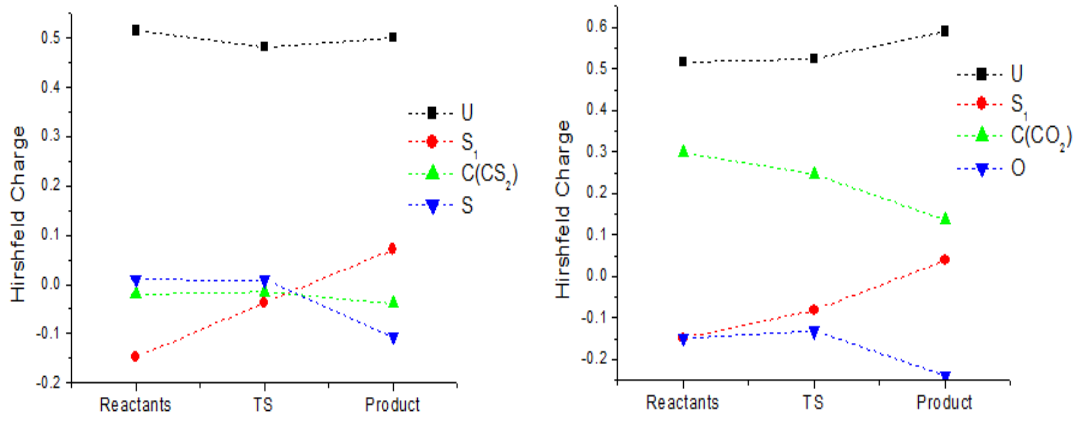

Fig. 8b. Evolution of the Hirshfeld charges during the three steps of the {[U(Cp)$_3$(SMe)] +CX$_2$} (X = S, O) reactions, in THF.

Finally, in the case of the CS_2 insertion, the calculated energy barriers in the solvent lead to the following ranking in the increasing order: $\Delta H^{\#}$ (Me) < $\Delta H^{\#}$ (^{i}Pr) < $\Delta H^{\#}$ (Ph) < $\Delta H^{\#}$ (^{t}Bu) in accordance with the steric crowding of the R groups of the SR ligand. According to Marçalo studies [74], the steric coordination numbers of the ligands are ranked as *Me (1.06)* < *^{i}Pr (1.22)* < *Ph (1.26)* < *^{t}Bu (1.50).*

3.2.2. Frontier molecular orbitals analysis of the {[U(Cp)$_3$(SR)] + CX$_2$} reactions

In order to investigate more thoroughly the reactivity of the monothiolate complexes towards the CS_2 and CO_2 molecules, a molecular orbital (MO) analysis was carried out for the transition states of the{[U(Cp)$_3$(SR)] + CX$_2$} reactions (R = Me, ^{i}Pr, Ph, ^{t}Bu and X = S, O). The comparative diagram of α–spin MOs of the transition state for the representative case ({[U(Cp)$_3$(S^{i}Pr)] + CX$_2$} reactions) is represented in Figure 6, showing the contributions of Cp_3, U, SR and CO_2 or CS_2 fragments (percentages % (Cp_3/U/SR/CO_2(or CS_2)). For the system with R = Me, see the Supporting Information SI.6.

For the {[U(Cp)$_3$(S^{i}Pr) + CO_2} reaction, the left side of the diagram shows that the highest occupied α spin–orbitals, i.e., SOMO, SOMO–1 are essentially metallic, with a strong f orbital character as indicated by the percentage orbital composition % (Cp_3/U/SR/CO_2 (or CS_2). This uranium contribution drops sharply in lower occupied MOs (SOMO–2 with 19%, SOMO–3 with 17.2%) which exhibit, on the contrary, a significant participation of the Cp ligands (more than 60% weight). A slight contribution of the reactive CO_2 molecule orbitals (around 1%), appears in SOMO–2. Concerning the vacant MOs, the important metallic character in the LUMO and LUMO+1 (94 %) decreases as one goes up in energy with a very weak contribution of the ligands surrounding the uranium atom.

Concerning the second reaction, i.e. {[U(Cp)$_3$(S^{i}Pr)] + CS_2} represented in the right part of the diagram (Figure 6), the same trend is found with the two higher SOMOs and the two lower LUMOs being essentially metallic (80–90%), with a strong f orbital character.

In the right part of the diagram, the contribution of the metallic centre orbitals (in particular the 5f ones) is dominating in the frontier MOs LUMO, LUMO+1, SOMO and SOMO–1. Unlike the reaction with CO_2, there is a substantial contribution from CS_2 orbitals in LUMO+1 (8.0%) that rises up to 8.3% in LUMO+2. The diagram shows a minor contribution of the orbitals of the thiolate ligand SR orbitals (approximately 2.0% in LUMO and LUMO+1) which increases in SOMO–2 (more than 18%), while the OA of Cp ligands are absent in the MOs except in LUMO+3 (14.4%) and SOMO–3 where it becomes very important (60.3 %).

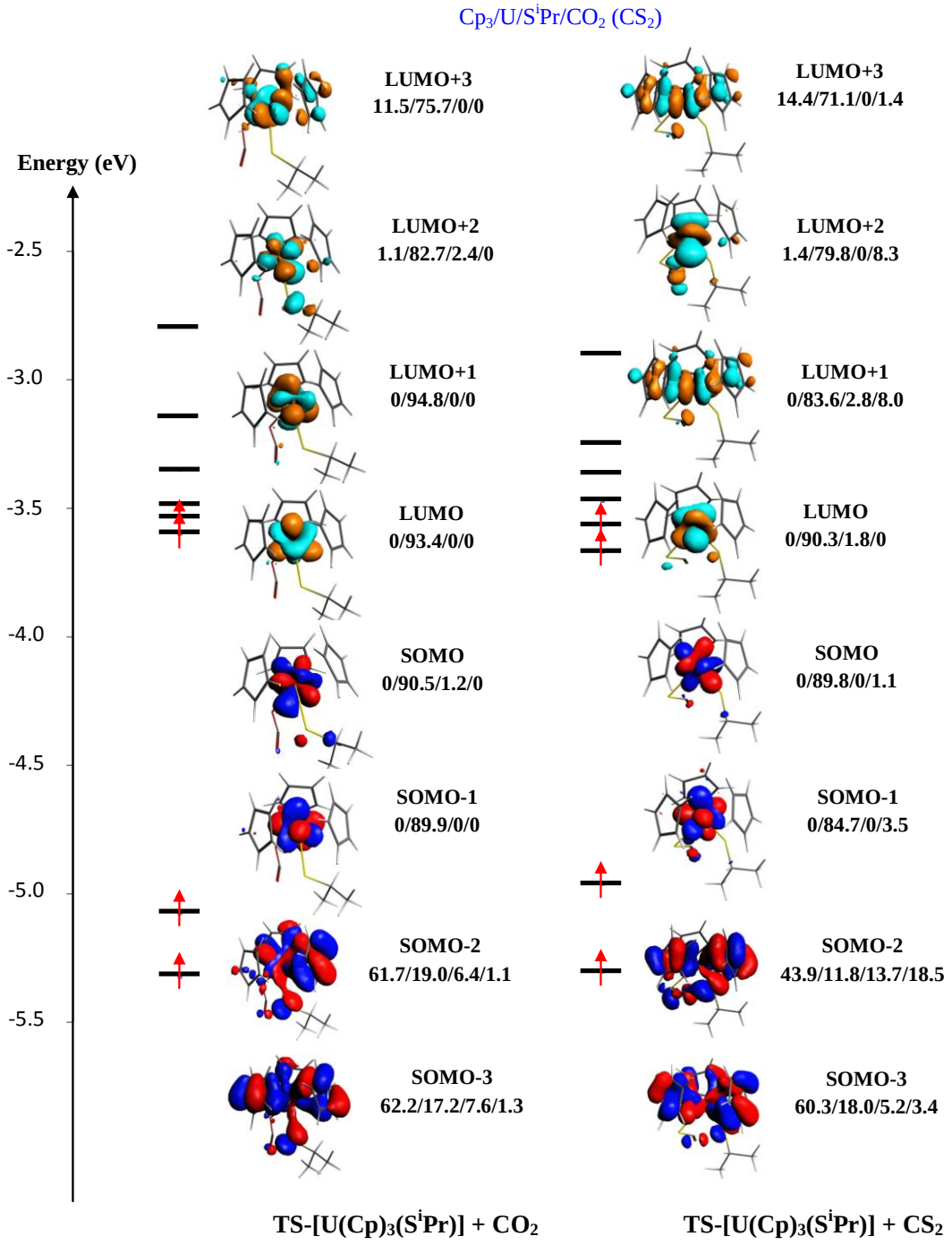

Fig. 6. Comparative diagram of α–spin MOs of the transition state of the {[$U(Cp)_3(S^iPr)$] + CX_2} reactions (X = O at the left of the figure and X = S at the right of the figure) in THF. The percentage weights give the contributions of the Cp, U, SR and CX_2 fragments of the TS species to the MOs (Contour values: 0.03 au).

3.2.3. Nalewajski–Mrozek analysis of the {[U(Cp)$_3$(SR)] + CX$_2$} reactions

In order to investigate the evolution of the atom–atom interactions during the insertion processes, the results of the NMBO analysis for the reactions with CS_2 are given in Table 5 (those of the reactions with CO_2 are given in the Supporting Information SI.7).

Table 5

NMBO bond orders in TS and products of the {[U(Cp)$_3$(SR)] +CS_2} reactions, calculated in THF.

Complex	Species	U−S$_1$	C$_2$−S$_2$	C$_2$−S$_3$	C$_2$−S$_1$	U−S$_2$	U−S$_3$
(**1**)	TS	0.814	1.543	1.461	0.348	0.588	–
	Product	–	1.269	1.445	1.174	0.710	0.473
(**2**)	TS	0.859	1.471	1.890	0.391	0.643	–
	Product	–	1.265	1.437	1.188	0.718	0.469
(**3**)	TS	0.663	1.390	1.815	0.520	0.699	–
	Product	–	1.271	1.469	1.122	0.709	0.487
(**4**)	TS	0.956	1.375	1.774	0.374	0.747	–
	Product	–	1.253	1.435	1.196	0.725	0.478

We note that the bond indices of U−S1 and C2−S2 bonds decrease to reach an average value of 0.80 and 1.50 respectively in the transition state, in parallel with the increase of their bond lengths. On the other hand, a weak bond between the central metal and one of the sulfur atoms of the reactive molecule CS_2 begins to form with a U−S2 NMBO value close to 0.60 in the transition states to reach the average value of 0.70 in the final products. Meanwhile a bond between the C atom of CS_2 and the sulfur atom of [U(Cp)$_3$(SR)] starts to be formed with an NMBO of 0.40 in the TS. These variations in bond indices during the insertion reactions are in agreement with those of the corresponding bond lengths, a low NMBO corresponding to a large bond length. The final products present simple bonds with NMBO values all larger than 1, except for the sulfur atoms of CS_2 bound to uranium, i.e. U−S2 and U−S3 for which the bond orders are close to 0.70 and 0.50 respectively. Figure 7a summarizes this process for the representative cases of the {[U(Cp)$_3$(SR)] + CS_2} reactions (R = Me, ^{i}Pr).

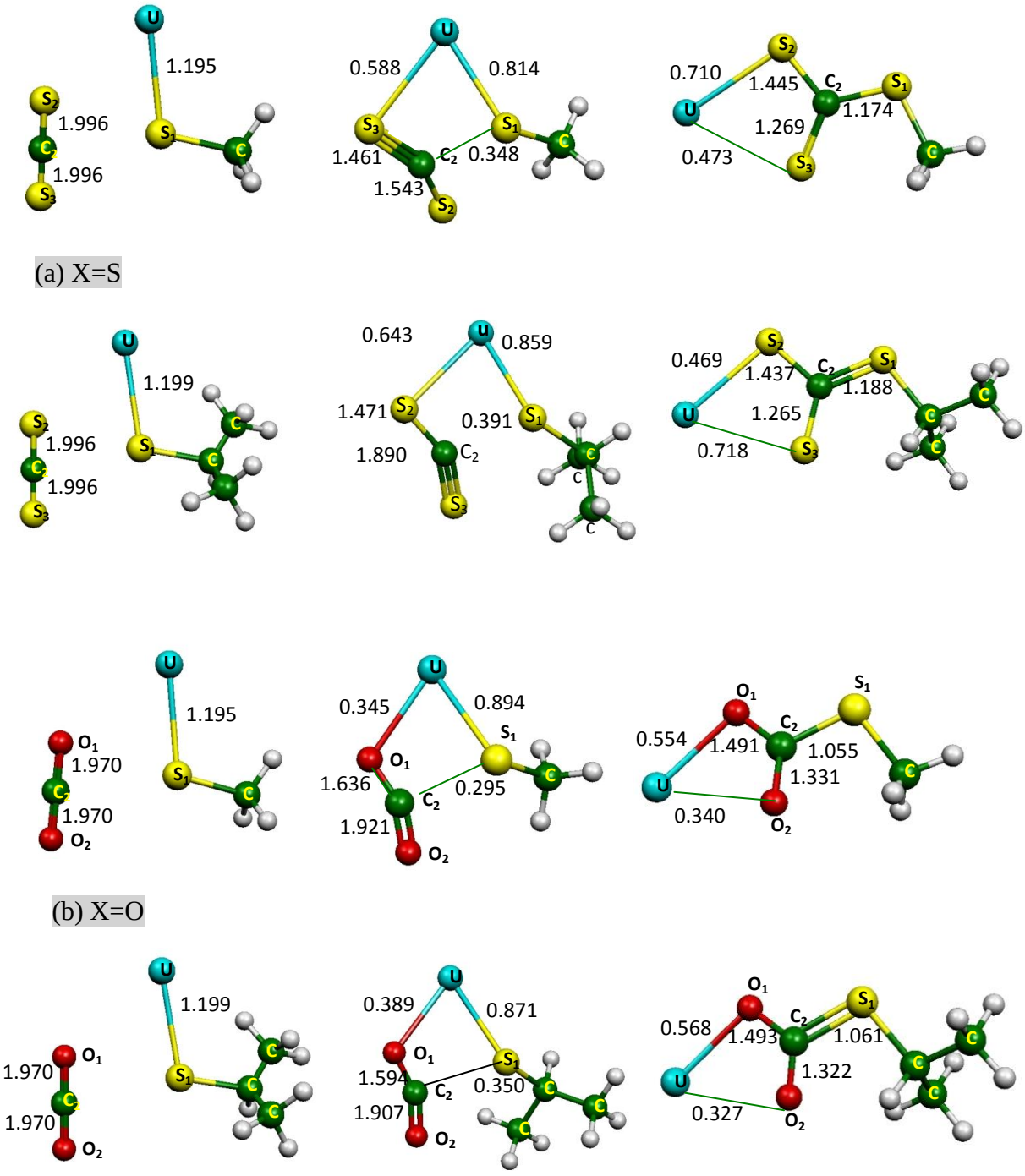

Fig. 7. Nalewajski−Mrozek bond orders of the different species of the {[U(Cp)$_3$(SR)] + CX$_2$} (R = Me, ^{i}Pr) reactions, (R= Me at the top of the figure and R = ^{i}Pr at the bottom of the figure, (a) X = S, (b) X = O), computed in the THF solvent.

For the case of CO_2, the NMBO analysis of the {[$U(Cp)_3(SR)$] + CO_2} reactions reveals the same tendency for all the insertion reactions of CO_2 into the U–S bond of these complexes. When going from the reactants towards the TS, the bond indices of U–S, C2–O1 and C2–O2 decrease, the two last bonds becoming different in the TS. As an example, during the reaction of **1** with CO_2 (see Figure 7b), the NMBO values vary from 1.195 (for U–S), 1.970 (for C2–O1and C2–O2) to 0.894, 1.636 and 1.921 in the TS, respectively. In the second step of the reaction, the evolution towards the product occurs by the insertion of the CO_2 molecule with the breaking of the U–S bond and the creation of two bonds between U and both O atoms of CO_2 (one shorter than the other). Another C–S bond is formed corresponding to a NMBO value changing from 0.295 in the TS to 1.055 in the product. In this final product, insertion into the U–S bond corresponds to the two NMBO values of 0.554 and 0.334 for the two U–O bonds.

3.3. Redox properties of the monothiolate uranium complexes [U(Cp)$_3$(SR)]

We consider now the redox properties of the complexes under consideration. The half−wave reduction potentials of complexes **2** and **3** have been determined experimentally by electrochemistry measurements [53,75] but not those of [$U(Cp)_3$(SMe)] (**1**) and [$U(Cp)_3(S^tBu)$] (**4**). In order to estimate the half−wave reduction potentials of these two latter monothiolate complexes we also undertook a study of the redox properties of the triscyclopentadienyl complexes [$U(Cp)_3$(X)] X = Cl, O^iPr, BH_4 and NEt_2 (electrochemical potentials relative to the U^{III}/U^{IV} systems of the latter species being measured). The geometries optimizations of the uranium(III) anionic complexes $[U(Cp)_3(SR)]^-$ have been carried out at the same level of theory as for the neutral U(IV) counterparts, considering their highest spin state $5f^3$ (see Cartesian coordinates and geometries of these U(III) anionic species in Supporting Information SI.8). As an example, the structure with some geometrical parameters of the complex [$U(Cp)_3$(SMe)] (**1**) and the corresponding anion are given in Figure 9.

The U(IV) → U(III) reduction process of the neutral complexes induces a significant increase of the calculated bond distances between the central metal and its neighbors. As one can see on the Figure 9, this lengthening of the U–S bond is equal to 0.13 Å (from 2.668 Å to 2.800 Å) for the isolated molecule **1** and to 0.15 Å in solution, whereas for the U–Cp(centroid) distances, the average variation is of 0.05 Å. This bond lengthening is in line

with the ionic radius increase by 0.135 Å for the U^{3+} relatively to U^{4+} ions [76]**.** The other parameters as the C−C and C−H bond lengths of the ligands and the centroid−U−centroid and centroid−U−S angles are not affected by the reduction of the neutral uranium(IV) complex since the variations do not exceed 0.02 Å for the distances and 1° for the angles.

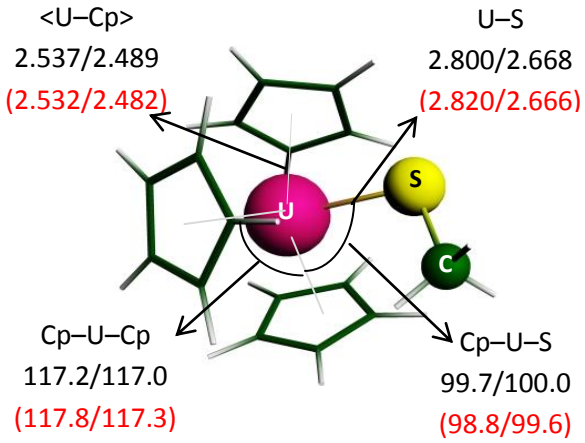

Fig. 9. Optimized geometries of the two U(III/IV)species of the $[U(Cp)_3(SMe)]$ **(1)** complex in the gas phase and in THF (in red). Left values for U(III) and right for U(IV) complexes.

The total bonding energies (TBEs) calculated for all species allow the determination of the electron affinities (EAs). In all cases, the EAs were computed according to the "ΔE method", that is the difference between the TBEs of the compounds and their reduced forms at their optimized geometries. The calculations have been carried out at the ZORA/BP86 level using both the TZP basis set and the more extended TZ2P one. The effects of the spin−orbit coupling were taken into account through 'single point' calculations using the previously optimized geometries. The computed TBE values are given in Supporting Information SI.9.

The EAs calculated in the gas phase and in solution (THF), for all the complexes at the same level of theory, are given in Table 7. In this table are displayed the results by using the more extended ADF/ZORA basis set, namely the TZ2P (triple zeta) that includes two functions of polarization. The columns with SO acronym correspond to the values of EAs which take into account spin–orbit coupling, whereas, in the last column of Table 7, are displayed the experimental half–wave reduction potentials of the neutral uranium(IV) complexes, ($E_{1/2}$ vs. $[Cp_2Fe]^{+/0}$) measured in volts in THF [53,75].

Table7

ZORA/BP86/TZ2P Computed Electron Affinities (in eV) EA calculated in the gas phase without and with spin−orbit coupling (SO) and in THF (THF+SO).

Complex	EA/eV	EA(SO)/eV	EA(THF+SO)/eV	$-E_{1/2}$/V
$U(Cp)_3(SMe)$	1.442	1.422	2.759	*
$U(Cp)_3(S^iPr)$	1.309	1.571	2.673	2.026
$U(Cp)_3(SPh)$	1.504	1.722	3.531	1.900
$U(Cp)_3(S^tBu)$	1.466	1.445	3.280	*
$U(Cp)_3(O^iPr)$	0.931	1.118	1.068	2.385
$U(Cp)_3(NEt_2)$	0.956	1.112	1.197	2.382
$U(Cp)_3(BH_4)$	1.291	1.611	3.121	1.995
$U(Cp)_3(Cl)$	1.405	1.802	3.637	1.875

*Systems not characterized (no measured values of $E_{1/2}$)

As expected, all the EAs are positive, going from 0.931 to 1.504 eV in the gas phase, and from 1.118 to 1.722 eV including the spin-orbit coupling corrections. This shows well the better stability of the anionic U(III) species relatively to their neutral U(IV)precursors. It is noted that the alkoxide derivative, $[U(Cp)_3(O^iPr)]$, having the smallest reduction half–wave potential (−2.385 V), exhibits the smallest EA (1.118 eV), thus making this compound the most difficult to reduce. On the contrary, its chloride congener $[U(Cp)_3(Cl)]$ proves to be the easiest to undergo a reduction, with the largest EA (1.802 eV) corresponding to the lowest potential (−1.875 V). In addition, it can be seen that spin–orbit coupling affects differently the TBEs of the neutral and anionic species, in their triplet and quartet states respectively, the latter compounds undergoing an energy lowering of 2.5 eV on average, whereas it is of 2.2 eV for the uranium(IV) complexes. In order to simulate the experimental conditions, solvent effects must be taken into account. The latter and spin–orbit corrections lead to significant variations of EAs. Moreover, it is interesting to note that relative ordering of the EAs of the uranium(IV) complexes in the gas phase can be changed in solution, as it is the case for **2** and **4**.

A very nice linear correlation is obtained between the computed electron affinities calculated in THF including the spin−orbit corrections and the available experimental half−wave reduction potentials $-E_{1/2}$, the correlation coefficient of the linear regression being equal to 0.99 with a slope of −0.202 (Figure 10).

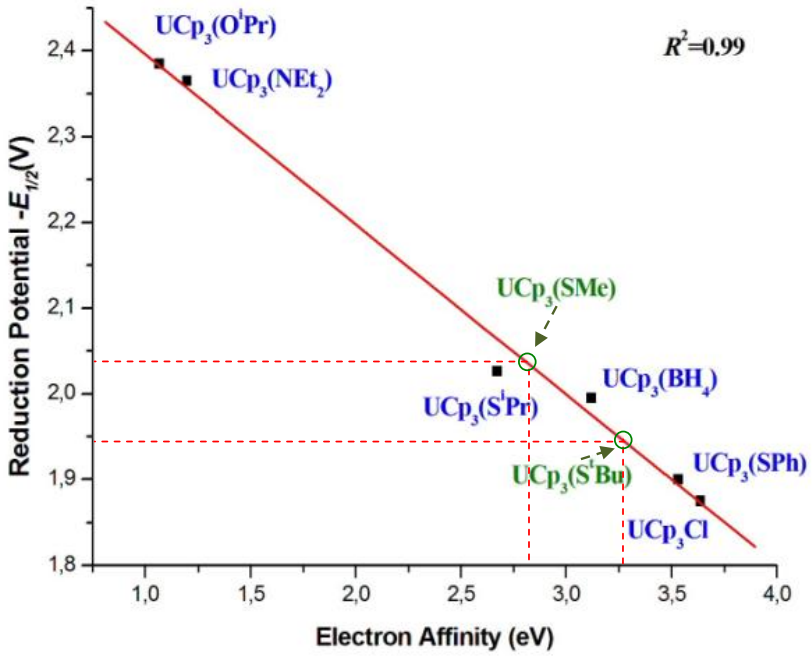

Fig. 10. Linear correlation between the computed electron affinities and the experimental half−wave reduction potentials $E_{1/2}$ for the $[U(Cp)_3(X)]$ complexes in THF.

We noted that the neglect of the spin−orbit correction leads to a worsening of the correlation between the EA (THF + SO) and the $E_{1/2}$, i.e. the R^2 coefficient varies from 0.99 to 0.90. This result is in agreement with our precedent works [67–69] and with a Shamov and Schreckenbach study [70], showing that spin−orbit corrections to the An(VI)/An(V) reduction potentials of the actinyl complexes $[AnO_2(H_2O)_5]^{n+}$ (An = U, Np and Pu) are essential to reproduce experimental results. Finally, it is worth noting that the use of the less extended TZP basis set slightly worsens the correlation between EA and $E_{1/2}$, with the R^2 factor being equal to 0.97.

This good correlation permits to estimate the half−wave reduction potentials of the two monothiolate complexes $[U(Cp)_3(SMe)]$ (**1**) and $[U(Cp)_3(S^tBu)]$ (**4**), not experimentally measured. Indeed, on the basis of the linear regression of Figure 10 and the computed EAs of

1 and **4**, respectively 2.76 eV and 3.28 eV, we can deduce the reduction potentials, $E_{1/2}\{U(Cp)_3(SMe)\} = -2.04$ V and $E_{1/2}\{U(Cp)_3(S^tBu)\} = -1.94$ V.

The good correlation $E_{1/2}$ *vs.* EAs confirms well the role of the electron donating ability of the X ligand in the redox properties, the more electron donor ligand leading to a complex exhibiting a smaller electron affinity as given by the following classification of the Hammett constants: $Cl < BH_4 < SPh < S^iPr < SMe < NEt_2 < O^iPr$ [77].

4. Conclusion

In the present work, new insights into the reactivity and the redox behavior of a series of triscyclopentadienyl monothiolate uranium(IV) complexes have been presented. In the first part of this study, the small molecules CS_2 and CO_2 insertion into the U–S bond of the triscyclopentadienyl monothiolate uranium(IV) complexes, i.e. $[U(Cp)_3(SR)]$ (R = Me (**1**), ^{i}Pr (**2**), Ph(**3**)and ^{t}Bu (**4**)) was investigated using relativistic ZORA/BP86 calculations taking account the solvent effects via the COSMO approach. The optimized geometries of the reactants are found in good agreement with the available X–ray structures. The structures of the transition states and products have been determined and characterized by Linear Transit (LT) and Intrinsic Reaction Coordinate (IRC) calculations. The $[U(Cp)_3(S^tBu)]$ complex presents the highest activation barrier in both reactions with CO_2 and CS_2, while $[U(Cp)_3(SMe)]$ is found most reactive, following the classification order of the steric hindrance constants of the R ligand. Finally, the computed activation barriers of these reactions also show that the CO_2 insertion into the U–S bond of the monothiolate complexes is easier than that of CS_2, in agreement with the experimental observations. This different reactivity of CO_2 and CS_2 is explained by the highest electronegativity of oxygen compared to that of sulfur leading to a strong electrostatic interaction between oxygen and uranium, then to the initial coordination of CO_2 to the central metal, before the migration of the SR group. The Hirshfeld analysis shows that the insertion of CO_2 is also supported by the electrostatic attraction between the positively charged carbon atom and the negatively charged sulfur atom with the SR ligand, which leads to the formation of U–O bonds more ionic than U–S ones.

In the second part of this work, with the aim of estimating the reduction potentials of $[U(Cp)_3(SMe)]$ and $[U(Cp)_3(S^tBu)]$ compounds, the redox properties of the monothiolate complexes and of a series of $[U(Cp)_3(X)]$ compounds (X = Cl, BH_4, NEt_2 and O^iPr) for which the experimental reduction potentials are available, have been investigated. The good linear correlation obtained ($R^2 = 0.99$) between the calculated electron affinities and the half–wave

reduction potentials allowed to estimate the reduction potentials of complexes **1** and **4**, which were not determined by electrochemistry.

Conflicts of Interest

The authors declare no conflicts of interest.

Acknowledgments

The authors acknowledge the financial support from the Algerian Project PRFU n° B00L01UN160420190019.Computing facilities were provided by ASELKAM Computer Center (UMMTO, Algeria). The authors are grateful to GENCI-IDRIS and GENCI-CINES for an allocation of computing time (Grant No. 2022−080649).

Supporting Information

SI.1: Optimized coordinates for isolated $[U(Cp)_3(SR)]$ molecules
SI.2: Optimized coordinates of TS and products of $\{[U(Cp)_3(SR)] + CS_2\}$ reactions
SI.3: Energy profiles of the $\{[U(Cp)_3(SR)] + CX_2\}$(X = ^{i}Pr, Ph, ^{t}Bu) reactions
SI.4: Energy profiles of the $\{[U(Cp)_3(SR)] + CO_2\}$ reactions in THF
SI.5: Hirshfeld Analysis in the gas phase
SI.6: Molecular Orbitals for the $\{[U(Cp)_3(SMe)] + CX_2\}$(X = S, O) reactions
SI.7: NMBO of the all species of the $\{[U(Cp)_3(SR)] + CO_2\}$ reactions
SI.8: Cartesian coordinates of the anionic $[U(Cp)_3(SR)]^-$ complexes
SI.9: TBEs of anionic and neutral species of $[U(Cp)_3(X)]$ (X = SR, Cl, BH_4, NEt_2, O^{i}Pr)

References

[1] T.J. Marks, R.D. Ernst, in G. Wilkinson, F.G.A. Stone and E.W. Abel (eds), Comprehensive organometallic chemistry, Vol. 3, Pergamon, Oxford, 1982, Chapter 21.
[2] W.J. Evans, J.R. Walensky, J.W. Ziller, A.L. Rheingold, Insertion of carbodiimides and organic azides into actinide−carbon bonds, Organometallics 28(2009) 3350−3357.
[3] P.J. Fagan, J.M. Manriquez, E.A. Maatta, A.M. Seyam, T.J. Marks, Synthesis and properties of bis(pentamethylcyclopentadienyl) actinide hydrocarbyls and hydrides. A new class of highly reactive f−element organometallic compounds, J. Am. Chem. Soc. 103 (1981) 6650−6667.
[4] J.M. Manriquez, P.J. Fagan, T.J. Marks, Insertion of carbon monoxide into metal−nitrogen

bonds. Synthesis, chemistry, structures, and structural dynamics of bis(pentamethylcyclopentadienyl) organoactinide dialkylamides and η^2-carbamoyls, J. Am. Chem. Soc. 100 (1978) 3939−3941.

[5] K.G. Moloy, T.J. Marks, The insertion of carbon dioxide into actinide alkyl and hydride bonds, Inorg. Chim. Acta 110 (1985) 127−131.

[6] M. Ephritikhine, Recent advances in organoactinide chemistry as exemplified by cyclopentadienyl compounds, Organometallics 32 (2013) 2464−2488.

[7] M. Ephritikhine, Molecular actinide compounds with soft chalcogen ligands, Coord. Chem. Rev. 319 (2016) 35−62.

[8] F. Kias, F. Talbi, A. Elkechai, A. Boucekkine, C-F bond breaking by bare actinide monocations in the gas phase: A relativistic DFT study, Comp. Theo. Chemistry, 1118 (2017) 133−143.

[9] K.C. Jantunen, C.J. Burns, I. Castro−Rodriguez, R.E. Da Re, J.T. Golden, D.E. Morris, B.L. Scott, F.L. Taw, J.L. Kiplinger, Thorium(IV) and uranium(IV) ketimide complexes prepared by nitrile insertion into actinide−alkyl and −aryl bonds, Organometallics 23 (2004) 4682−4692.

[10] J.A. Pool, B.L. Scott, J.L. Kiplinger, A new mode of reactivity for pyridine N−oxide: C−H activation with uranium(IV) and thorium(IV) bis(alkyl) complexes, J. Am. Chem. Soc. 127 (2005) 1338−1339.

[11] J.G. Brennan, R.A. Andersen, A. Zalkin, Chemistry of trivalent uranium metallocenes: Electron−transfer reactions with carbon disulfide. Formation of $[(RC_5H_4)_3U]_2$[.mu. −.eta.1.eta.2−CS_2], Inorg. Chem. 25 (1986) 1756−1760.

[12] J.G. Brennan, R.A. Andersen, A. Zalkin, Chemistry of trivalent uranium metallocenes: Electron−transfer reactions. Synthesis and characterization of $[(MeC_5H_4)_3U]_2E$ (E = S, Se, Te) and the crystal structures of hexakis (methylcyclopentadienyl) sulfidodiuranium and tris(methylcyclopentadienyl) (triphenylphosphine oxide) uranium, Inorg. Chem. 25 (1986) 1761−1765.

[13] J.C. Berthet, J.F. Le Maréchal, M. Nierlich, M. Lance, J. Vigner, M. Ephritikhine, Synthesis and crystal structure of the oxo−bridged bimetallic organouranium complex $[(Me_3SiC_5H_4)_3U]_2$[μ−O], J. Organomet. Chem. 408 (1991) 335−341.

[14] P.C. Leverd, M. Ephritikhine, M. Lance, J. Vigner, M. Nierlich, Triscyclopentadienyl uranium thiolates and selenolates, J. Organomet. Chem. 507 (1996) 229−237.

[15] C. Rodriguez, K. Olsen, P. Gantzel, K. Meyer, Uranium complexes supported by an

aryloxide functionalized triazacyclononanemacrocycle: Synthesis and characterization of a six−coordinate U(III) species and insights into its reactivity, Chem. Commun. (2002) 2764−2765.

[16] F.G.N. Cloke, P.B. Hitchcock, Reversible binding and reduction of dinitrogen by a uranium(III) pentalene complex, J. Am. Chem. Soc. 124 (2002) 9352−9353.

[17] I. Castro−Rodriguez, H. Nakai, L.N. Zakharov, A. L Rheingold, K. Meyer, A linear, O−**c**oordinated η^1−CO_2 bound to uranium, Science 305 (2004) 1757−1759.

[18] H. Nakai, I.C. Rodriguez, N.L. Zhakarov, A.L. Rheingold, K. Meyer, Synthesis and characterization of N−heterocyclic carbene complexes of uranium(III), Inorg. Chem., 43 (2004) 855−857.

[19] F. Talbi−Ingrachen, F. Talbi, F. Kias, A. Elkechai, A. Boucekkine, C. Daul, DFT investigation of methane metathesis with L_2AnCH_3 actinide complexes catalysts (L = Cl, Cp, Cp*; An = Ac, Th, Pa, U, Np, Pu), Comp. Theo. Chemistry, 1138 (2018) 123−134.

[20] O.T. Summerscales, F.G.N. Cloke, P.B. Hitchcock, J.C. Green, N. Hazari, Reductive cyclotrimerization of carbon monoxide to the deltate dianion by an organometallic uranium complex, Science 311 (2006) 829−831.

[21] O.T. Summerscales, F.G.N. Cloke, P.B. Hitchcock, J.C. Green, N. Hazari, Reductive cyclotetramerization of CO to squarate by a U(III) complex: The X−ray crystal structure of $[(U(\eta-C_8H_6\{Si^iPr_3-1,4\}_2)(\eta-C_5Me_4H)]_2(\mu-\eta^2-\eta^2-C_4O_4)$, J. Am. Chem. Soc. 128 (2006) 9602−9603.

[22] A.S. Frey, F.G.N. Cloke, P.B. Hitchcock, I.J. Day, J.C. Green, G. Aitken, Mechanistic studies on the reductive cyclooligomerisation of CO by U(III) mixed sandwich complexes; the molecular structure of $[(U(\eta-C_8H_6\{Si^iPr_3-1,4\}_2)(\eta-Cp^*)]_2(\mu-\eta^1:\eta^1-C_2O_2)$, J. Am. Chem. Soc. 130 (2008) 13816−13817.

[23] O.T. Summerscales, A.S. Frey, F.G.N. Cloke, P.B. Hitchcock, Reductive disproportionation of carbon dioxide to carbonate and squarate products using a mixed−sandwich U(III) complex, Chem. Commun. (2009) 198−200.

[24] O.P. Lam, F.W. Heinemann, K.C.R. Meyer, Chim. A new diamantane functionalized tris(aryloxide) ligand system for small molecule activation chemistry at reactive uranium complexes, Comp. Theo. Chemistry,13 (2010) 803−811.

[25] W.J. Evans, N.A. Siladke, J.W. Ziller, Synthesis and reactivity of a silylalkyl double tuck−in uranium metallocene $[(\eta^5:\eta^1-C_5Me_4SiMe_2CH_2)_2U]$ and its conversion to bis(tethered) metallocenes, Chem. Eur J. (2010) 796−797.

[26] S.M. Mansell, N. Kaltsoyannis, P.L. Arnold, Small molecule activation by uranium tris(aryloxides): Experimental and computational studies of binding of N_2, coupling of CO, and deoxygenation insertion of CO_2 under ambient conditions, J. Am. Chem. Soc. 133 (2011) 9036−9051.
[27] D.M. Su, H.X. Cai, X.J. Zheng, S. Niu, Q.J, Pan, Theoretical design and exploration of low−valent uranium metallocenes *via* manipulating cyclopentadienyl substituent, theory, Comp. Theo. Chemistry, 1195 (2012) 113107-11314.
[28] W. Ding, W. Fang, Z. Chai, D. Wang, Trivalent uranium complex as a catalyst to promote the functionalization of carbon dioxide and carbon disulfide: A computational mechanistic study, J. Chem. Theory Comput. 8 (2012) 3605−3617.
[29] B.M. Gardner, J.C. Stewart, A.L. Davis, J. McMaster, W. Lewis, A.J. Blake, S.T. Liddle, Homologation and functionalization of carbon monoxide by a recyclable uranium complex, Proc. Natl. Acad. Sci. U.S.A. 109 (2012) 9265−9270.
[30] V. Mougel, C. Camp, J. Pécaut, C. Copéret, L. Maron, C.E. Kefalidis, M. Mazzanti, Siloxides as supporting ligands in uranium(III)−mediated small−**m**olecule activation, Angew. Chem. Int. Ed. 51 (2012) 12280−12284.
[31] N. Tsoureas, O.T. Summerscales, F.G.N. Cloke, S.M. Roe, Steric effects in the reductive coupling of CO by mixed−**s**andwich uranium(III) complexes, Organometallics 32 (2013) 1353−1362.
[32] O. Cooper, C. Camp, J. Pécaut, C.E. Kefalidis, L. Maron, S. Gambarelli, M. Mazzanti, Multimetallic cooperativity in uranium−**m**ediated CO_2 activation, J. Am. Chem. Soc., 136 (2014) 6716−6723.
[33] E.M. Matson, A.T. Breshears, J.J. Kiernicki, B.S. Newell, P.E. Fanwick, M.P. Shores, J.R. Walensky, S.C. Bart, Trivalent uranium phenylchalcogenide complexes: Exploring the bonding and reactivity with CS_2 in the Tp^*_2UEPh series (E = O, S, Se, Te), Inorg. Chem. 53 (2014) 12977−12985.
[34] Y.R. Guo, N. Qu, Q.J. Pan, A theoretical probe for pentavalent bis−imido uranium complexes containing diverse axial substituents and equatorial donors: U−N multiple bond and structural/electronic properties, Comp. Theo. Chemistry, 1082 (2016) 21−28.
[35] L. Castro, L. Maron, Insight into the reaction mechanisms of $(MeC_5H_4)_3U$ with isoelectronic heteroallenes CS_2, COS, PhN_3, and PhNCO by DFT studies: A unique pathway that involves bimetallic complexes, Chem. –Eur. J., 18 (2012) 6610−6615.
[36] I. Castro−Rodriguez, K. Meyer, Carbon dioxide reduction and carbon monoxide

activation employing a reactive Uranium(III) complex, J. Am. Chem. Soc. 127 (2005) 11242−11243.

[37] N. Tsoureas, L. Castro, A.F.R. Kilpatrick, F. Geoffey N. Cloke and L. Maron, Controlling selectivity in the reductive activation of CO_2 by mixed sandwich uranium(III) complexes, Chem. Sci., 5 (2014) 3777−3788.

[38] J.M. Berg, R.H. Holm 4, Iron-sulfur proteins, Wiley−Interscience, New York, 1982.

[39] D. Coucouvanis, Use of preassembled iron/sulfur and iron/molybdenum/sulfur clusters in the stepwise synthesis of potential analogs for the Fe/Mo/S site in nitrogenase, Ace. Chem. Res. 24 (1991) 1−8.

[40] B.C. Wiegand, C.M. Friend, Model studies of the desulfurization reactions on metal surfaces and in organometallic complexes, Chem. Rev. 92 (1992) 491−504.

[41] I. Santos, N. Marques, A. Pires de Matos, Uranium (IV) bishydrotris (pyrazol−1−yl) boratothiolato derivatives, Inorg. Chim. Acta 139 (1987) 89−90.

[42] Z. Lin, C.P. Brock, T.J. Marks, Synthesis, structural characterization, and properties of the organothoriumalkylthiolate complex $[(CH_3)_5C_5]_2Th(SCH_2CH_2CH_3)_2$, Inorg. Chim. Acta 141 (1988) 145−149.

[43] K. Tatsumi, I. Matsubara, Y. Inoue, A. Nakamura, R.E. Cramer, G.J. Tagoshi, J.A. Golen, J.W. Gilje, A homoleptic uranium thiolate: Synthesis, structure, and fluxional behavior of $[Li(dme)]_4[U(SCH_2CH_2S)_4]$ and reaction with carbon disulfide, Inorg. Chem. 29 (1990) 4928−4938.

[44] S.D. Stults, R.A. Andersen, A. Zalkin, Chemistry of trivalent cerium and uranium metallocenes: Reactions with alcohols and thiols, Organometallics 9 (1990) 1623−1629.

[45] A. Domingos, A. Pires de Matos, I. Santos, Synthesis and characterization of the uranium alkylthiolate complex $U(SPri)_2(HBPz_3)_2$, Polyhedron 11 (1992) 1601−1606.

[46] D.L. Clark, M.M. Miller, J.G. Watkin, Synthesis, characterization, and x−ray structure of the uranium thiolate complex $U(S-2,6-Me_2C_6H_3)[N(SiMe_3)_2]_3$,Inorg. Chem. 32 (1993) 772−774.

[47] E.M. Matson, P.E. Fanwick, S.C. Bart, Formation of trivalent U–C, U–N, and U–S bonds and their reactivity toward carbon dioxide and acetone, Organometallics 30 (2011) 5753−5762.

[48] C. Lescop, T. Arliguie, M. Lance, M. Nierlich, M. Ephritikhine, Bispentamethylcyclopentadienyluranium(IV) thiolate compounds. Synthesis and reactions with CO_2 and CS_2, J. Organomet. Chem. 580 (1999) 137−144.

[49] F. Talbi, L. Castro, F. Kias, A. Elkechai, A. Boucekkine, M. Ephritikhine, Theoretical investigation of the reactivity of bispentamethylcyclopentadienyl uranium(IV) bisthiolate complexes with the heteroallene molecules CS_2 and CO_2, J. Organomet. Chem. 901 (2019) 120947−12058.

[50] R.F. Nalewajski, J. Mrozek, Modified valence indices from the two−particle density matrix, Int. J. Quantum. Chem., 51 (1994) 187−200.

[51] R.S. Mulliken, Electronic population analysis on LCAO–MO molecular wave functions, J. Chem. Phys., 23 (1955) 1883−1887.

[52] F.L. Hirshfeld, Bonded−atom fragments for describing molecular charge densities, Theor. Chim. Acta., 44 (1977) 129−138.

[53] A. Elkechai, A. Boucekkine, L. Belkhiri, M. Amarouche, C. Clappe, D. Hauchard, M. Ephritikhine. A DFT and experimental investigation of the electron affinity of the triscyclopentadienyluranium complexes Cp_3UX, Dalton Trans (2009) 2843−2849.

[54] P. Hohenberg, W. Kohn, Inhomogeneous electron gas, Phys. Rev. 136 (1964) B864−B871.

[55] W. Kohn, L. Sham, Self−**c**onsistent equations including exchange and correlation effects, J. Phys. Rev. 140 (1965) A1133−A1138.

[56] R.G. Parr, W. Yang, Density functional theory of atoms and molecules; Oxford University Press: Oxford, U.K., 1989.

[57] E. van Lenthe, E.J. Baerends, J. G. Snijders, The zero−order regular approximation for relativistic effects: The effect of spin−orbit coupling in closed−shell molecules, J. Chem. Phys. 101 (1994) 9783−9792.

[58] E. van Lenthe, A. Ehlers, E. J. Baerends, Geometry optimizations in the zero order regular approximation for relativistic effects**,** J. Chem. Phys. 110 (1999) 8943−8953.

[59] A. Klamt, Conductor−like screening model for real solvents: A new approach to the quantitative calculation of solvation phenomena, J. Phys. Chem. 99 (1995) 2224−2235.

[60] A. Klamt, V. Jonas, T. Bürger, J.C. Lohrenz, Refinement and parametrization of COSMO−RS, J. Phys. Chem. A 102 (1998) 5074−5085.

[61] ADF2017.103; SCM, Theoretical chemistry. Vrije University: Amsterdam, The Netherlands, 2017. http://www.scm.com.

[62] S.D. Vosko, L. Wilk, M. Nusair, Accurate spin–dependent electron liquid correlation energies for local spin density calculations: A critical analysis, Can. J. Chem. 58 (1990)

1200–1211.
[63] A.D. Becke, Density functional calculations of molecular bond energies, J. Chem. Phys. 84 (1986) 4524–4529.
[64] A.D. Becke, Density−functional exchange−energy approximation with correct Asymptotic behavior, Phys. Rev. A 38 (1988) 3098–3100.
[65] J.P. Perdew, Y. Wang, Accurate and simple analytic representation of the electron–gas correlation energy, Phys. Rev. B 45 (1992) 13244–13249.
[66] N. Kaltsoyannis, Recent developments in computational actinide chemistry, Chem. Soc. Rev., 32 (2003) 9−16.
[67] A. Elkechai, Y. Mani, A. Boucekkine, M. Ephritikhine, Density functional theory investigation of the redox properties of tricyclopentadienyl− and phospholyluranium(IV) chloride complexes, Inorg. Chem., 51 (2012) 6943−6952.
[68] A. Elkechai, F. Kias, F. Talbi, A. Boucekkine, Redox properties of biscyclopentadienyl uranium(V) imido−halide complexes: a relativistic DFT study, J. Mol. Model., 20 (2014) 2294−2304.
[69] F. Kias, F. Talbi, A. Elkechai, A. Boucekkine, D. Hauchard, J.C. Berthet, M. Ephritikhine, Redox properties of monocyclooctatetraenyluranium(IV) and (V) complexes: Experimental and relativistic DFT studies, Organometallics,36, 19 (2017) 3841−3853.
[70] G.A. Shamov, G. Schreckenbach, Density functional studies of actinyl aquo complexes studied using small−core effective core potentials and a scalar four−component relativistic method, J. Phys. Chem. A, 109 (2005) 10961−10974.
[71] C. van Wüllen, Spin densities in two−component relativistic density functional calculations: Noncollinear versus collinear approach, J. Comput. Chem., 23 (2002) 779−785.
[72] MOLEKEL4.3, P. Flükiger, H.P. Lüthi, S. Portmann and J. Weber, Swiss Center for Scientific Computing, Manno, Switzerland, 2000, http://www.cscs.ch.
[73] C. Gonzalez, H.B. Schlegel, An improved algorithm for reaction path following, J. Chem. Phys. 90 (1989) 2154–2161.
[74] J. Marçalo, A. Pires De Matos, A new definition of coordination number and its use in lanthanide and actinide coordination and organometallic chemistry, Polyhedron, 8 (1989) 2431−2437.

[75] C. Clappe, D. Sc. Thesis, Université de Paris VI, Paris, France, (1997).

[76] R.D. Shannon, Revised effective ionic radii and systematic studies of interatomic distances in halides and chalcogenides, Acta Crystallogr., Sect. A32 (1976) 751−767.

[77] L.P. Hammett, The effect of Structure upon the reactions of Organic Compounds. Benzene Derivatives, J. Am. Chem. Soc., 59 (1937) 96−103.